metals

MDPI

Article

Fatigue Damage Accumulation Modeling of Metals Alloys under High Amplitude Loading at Elevated Temperatures

Jarosław Szusta * and Andrzej Seweryn

Faculty of Mechanical Engineering, Bialystok University of Technology, 45C Wiejska Str., 15-351 Bialystok, Poland; a.seweryn@pb.edu.pl

* Correspondence: j.szusta@pb.edu.pl; Tel.: +48-085-746-9300; Fax: +48-085-746-9210

Received: 16 November 2018; Accepted: 3 December 2018; Published: 6 December 2018

Abstract: This article presents an approach related to the modeling of the fatigue life of constructional metal alloys working under elevated temperature conditions and in the high-amplitude load range. The article reviews the fatigue damage accumulation criteria that makes it possible to determine the number of loading cycles until damage occurs. Results of experimental tests conducted on various technical metal alloys made it possible to develop a fatigue damage accumulation model for the LCF (Low Cycle Fatigue) range. In modeling, the material's damage state variable was defined, and the damage accumulation law was formulated incrementally so as to enable the analysis of the influence of loading history on the material's fatigue life. In the proposed model, the increment of the damage state variable was made dependent on the increment of plastic strain, on the tensile stress value in the sample, and also on the actual value of the damage state variable. The model was verified on the basis of data obtained from experiments in the field of uniaxial and multiaxial loads. Samples made of EN AW 2024T3 aluminum alloy were used for this purpose.

Keywords: elevated temperature; low cycle fatigue; damage accumulation; uniaxial and multiaxial loading

1. Introduction

During operation, machine parts are frequently subjected to fatigue loading at elevated temperatures. Such operating conditions have an adverse effect on the materials' behavior. An elevated temperature accelerates wear processes and contributes to increasing the rate of fatigue crack propagation [1,2]. Aluminum alloys, e.g., EN AW 2024T3, are among the materials used to make constructions capable of working at an elevated temperature. It is widely used in the motorization and aviation industries, which place strong emphasis on ensuring high strength and light weight at the same time [3]. These features make it suitable for the manufacture of parts working in close proximity to combustion and jet engines where elevated temperature zones are present. In the work of Szusta and Seweryn [4,5], the influence of elevated temperature on the fatigue life of this material was tested. The authors demonstrated that strength parameters decreased as the test temperature increased. Based on the tests conducted, the authors determined the parameters of the Manson-Coffin fatigue life curve as a function of temperature:

$$\frac{\Delta\varepsilon_{eq}}{2} = \frac{\sigma_f'(T)}{E(T)}(2N_f)^{b(T)} + \varepsilon_f'(T)(2N_f)^{c(T)}, \quad (1)$$

where N_f is the number of cycles until failure; $E(T)$ is Young's modulus determined at temperature T; $\sigma_f'(T)$ and $\varepsilon_f'(T)$ are, respectively, coefficients of the elastic fatigue life curve and plastic fatigue life

curve for the analyzed temperature T; and $b(T)$ and $c(T)$ are, respectively, exponents of the elastic and plastic fatigue life curve for temperature T. Furthermore, based on observations of the material's cracking mechanisms at an elevated temperature, the authors proposed a semi-empirical model for estimating the material's fatigue life. In this model, it was accepted that the material's fatigue life drops as the test temperature (isothermal) increases. The lower the material's melting temperature, the more substantial this drop is. Moreover, it was assumed that there exists a limit temperature T_m at which the given material no longer has any immediate strength. Therefore, knowing the value of this temperature and the function defining the reduction in fatigue life as temperature increases, calculations of the number of cycles until crack initiation can be performed with engineering accuracy for a given temperature level and strain amplitude. For uniaxial tensile-compressive loads, the function of the temperature's influence on the material's fatigue life has been defined as follows:

$$N_f(T) = AT + B, \tag{2}$$

where A and B are material constants determined in periodical tensile-compression tests at temperature T.

In this model, the material constant B is a function of the material's recrystallization temperature T_m ($B = -AT_m$). The value of parameter A is calculated on the basis of the experimentally determined number of cycles to failure (obtained for a given load course at room temperature) related to the value of temperature difference: the material recrystallization and room temperature. Parameter A is determined from the following equation:

$$A\left(\frac{\Delta\varepsilon_{eq}}{2}\right) = -\frac{N_f\left(RT, \frac{\Delta\varepsilon_{eq}}{2}\right)}{(T_m - RT)}, \tag{3}$$

where $N_f\left(RT, \frac{\Delta\varepsilon_{eq}}{2}\right)$ is determined from Manson–Coffin–Basquiun equation at room temperature RT for the set total strain amplitude $\frac{\Delta\varepsilon_{eq}}{2}$.

Modified cast irons and cast steels, which are used in the manufacture of brake disks, are another group of materials that can be exploited at elevated temperatures. In the works of Samec et al. [6], Peve et al. [7], and Li et al. [8], the authors analyzed the fatigue life of the following materials: EN-GJS-500-7, EN-GJL-250, and Cr-Mo-V. Material cracking mechanisms were studied within the LCF range at temperature up to 700 °C, and the influence of temperature on the material's physical properties was defined.

Alloy steels are another group of materials used to make constructions which are exposed to the action of elevated temperatures. Here, some examples include 8Cr-2WvTa, (RAFM) JLF-1, or 617M steels, which are used to build thermoreactors and machine parts exposed to the action of high temperatures. In the works of Ishii et al. [9], Mariappan et al. [10], and Shankar et al. [11], the characteristics of these steels' cyclic properties were determined as a function of temperature. Degradation mechanisms of materials subjected to the action of fatigue loads and temperatures were analyzed. In the article by Ishii et al. [9], an approach to modeling fatigue life of the material was also presented, accounting for the influence of creep on the material's fatigue life:

$$\varepsilon_{eq}(N_f, T) = \varepsilon_e(N_f, T) + \varepsilon_{pl}(N_f, T) + \varepsilon_{cr}(N_f, T), \tag{4}$$

where ε_{eq} is the equivalent strain, ε_e is the elastic strain, ε_{pl} is the plastic strain, and ε_{cr} is the creep-induced strain.

Works by Nagode and Zingsheim [12] and Nagode and Hack [13] present the results of experimental tests performed on steels for work at elevated temperatures: 10 CrMo 9 10 and X22CrMoV121. Fatigue damage accumulation models of the material under non-isothermal conditions at elevated temperatures were developed on the basis of these results. These models were developed

for estimation of the fatigue life of materials which undergo changes of the load amplitude and temperature transient over the course of its exploitation. These models do not account for the influence of creep or hardening of the material on its fatigue life. The authors presented a stress and strain approach in which it is assumed that the instant working temperature will be accounted for. In models, stabilized hysteresis loops were described by means of the Ramberg–Osgood equation. The damage parameter P_{SWT} was identified similarly as in the SWT (Smith–Watson–Topper) model:

$$\begin{aligned} P_{SWT} &= \sqrt{\left(\sigma_f'^2(T_e)(2N_f)^{2b(T_e)} + \sigma_f'(T_e)E(T_e)\right)\varepsilon_f'(T_e)(2N_f)^{b(T_e)+c(T_e)}}, \text{ where} \\ \varepsilon_f'(T_e) &= \left(\frac{\sigma_f'(T_e)}{K'(T_e)}\right)^{\frac{1}{n'(T_e)}}, \\ c(T_e) &= \frac{b(T_e)}{n'(T_e)}, \end{aligned} \tag{5}$$

where T_e is the actual temperature; $\sigma'_f(T_e)$ and $b(T_e)$ are, respectively, the coefficient and exponent of the fatigue life curve at the tested temperature; $K'(T_e)$ and $n'(T_e)$ are, respectively, the coefficient and exponent of the cyclic hardening curve at the tested temperature; and $\varepsilon'_f(T_e)$ and $c(T_e)$ are, respectively, the coefficient and exponent of the plastic fatigue life curve.

Elements of gas turbines, e.g., rotor blades working under extremely difficult conditions, are also made from Inconel 718 alloy. Test results for this material was given in the work of Schlesinger et al. [14]. Here, a dispersion-hardening nickel-chromium alloy was analyzed with respect to fatigue loading at temperatures up to 650 °C. Similarly, in a different study [15], the same authors studied the Inconel 718 alloy. They proposed a model for estimation of the fatigue life of material working at elevated temperatures. The Manson–Coffin equation was used during modeling, in which parameters of the fatigue life curve were made functionally dependent on the structure and grain size in the given material G, test temperature T, and strength parameter S:

$$\frac{\Delta\varepsilon_{eq}(G,T,S)}{2} = \frac{\sigma_f'(G,T,S)}{E(T)}(2N_f)^{b(G,T,S)} + \varepsilon_f'(G,T)(2N_f)^{c(G,T)} \tag{6}$$

Materials adapted for manufacturing tools like casting molds and forging dies play an important role among materials intended for work at elevated temperature. In the study by Tunthawiroon et al. [16], the single-phase Co-29Cr-6Mo steel alloy, intended for aluminum casting molds, was tested. The study included analysis of the alloy's cracking mechanisms at temperatures up to 700 °C. A simple fatigue damage accumulation model at elevated temperatures was also proposed based on the Arrhenius equation:

$$D = N_f^{-1} = A\exp(Q/RT) \tag{7}$$

where N_f is the number of cycles until crack initiation, T is the test temperature, R and A are material constants, and Q is the activation energy.

Similarly, the works of Gopinath et al. [17] and He et al. [18] present the results of experimental tests conducted on 720Li and HAYNES HR-120 superalloys within the low-cycle fatigue range at temperatures up to 980 °C. The material was tested under uniaxial tensile-compressive loads. The mechanisms accompanying the cracking of these materials were defined.

ACI HH50 austenitic stainless steels can also work at elevated temperatures. The results given in the work by Kim and Jang [19] can serve as evidence of this. Due to its high resistance to elevated temperatures, high fatigue strength, and resistance to pitting and corrosion, the material in question finds applications in parts of combustion engines and power unit structures of nuclear power plants. The paper investigates the material's degradation mechanisms and presents a model estimating fatigue

life in the LCF range. The model assumes that fatigue crack initiation will occur when damage reaches a limit value given by the following function:

$$\begin{aligned} &\left(\frac{N_f}{N_0}\right)\left(\frac{\Delta\varepsilon_p}{\Delta\varepsilon_{p0}}\right)\sinh\left(\frac{\Delta\varepsilon_p}{\Delta\varepsilon_{p0}}\right) = 1, \quad \text{where} \\ &N_0 = \frac{\alpha\nu C}{\dot{\varepsilon}_0 \exp\left(\frac{Q}{RT}\right)}, \\ &\Delta\varepsilon_{p0} = \frac{\dot{\varepsilon}_0 \exp\left(\frac{-Q}{RT}\right)}{\nu}, \end{aligned} \tag{8}$$

where α is the material constant associated with dislocation movement over the course of the material loading process, ν is the frequency of load change during the test, $\dot{\varepsilon}_0$ and C are material constants independent of test temperature, Q is activation energy, R is the gas constant, and T is the test temperature.

The non-linear creep damage accumulation model under uniaxial loads at elevated temperatures (700 °C) that was also developed on the basis of tests performed on stainless steel X-8-CrNiMoNb-16-16 was presented by Pavlou 2001 [20]. The model was developed and verified by other researchers. In the work of Grell et al. [21], attempts have been made to estimate durability under the conditions of uniaxial isothermal loads (constant and incremental) at elevated temperatures using the dependencies proposed by Pavlou 2001 [20]. The work demonstrates greater accuracy in predicting durability with the use of non-linear models of the accumulation of defects in relation to linear models.

Titanium alloys are the next group of materials used to manufacture components working at elevated temperatures. One study [22] analyzes the influence of different methods of the surface hardening of the Ti-6Al-4V titanium alloy on the fatigue life of this material under uniaxial tensile-compressive loading conditions at temperatures up to 555 °C. The influence of temperature on the evolution of the cyclic properties of the TNB-V2 titanium alloy is also presented in the work [23]. Specimens of the material were subjected to constant-amplitude strains within the low-cycle loading range at temperatures within the range of 550–850 °C. Due to its good mechanical properties at elevated temperatures, this alloy finds applications in motorization and aviation and in engine parts. The authors tested the material within the entire safe temperature range, and determined that, in the case of this alloy, the Manson–Coffin fatigue life model does not allow for the prediction of the material's fatigue life at elevated temperatures due to the length of the phase between fatigue crack initiation and its propagation.

The fatigue damage accumulation model proposed in this paper was designed to predict the fatigue life of the material operated at elevated temperatures. The concept of elevated temperature can be defined here, according to the works by Chen et al. [24], as the temperature corresponding to two-thirds of the melting point of the bulk material T_c. In most cases, as temperature increases, a material's strength and fatigue properties are reduced in a predictable manner until a certain threshold temperature value is reached [25]. Under these conditions, the operation of technical machinery may be safe when the material's response to loading conditions and the working environment are known. However, if the conventional upper threshold of elevated temperature is crossed even slightly, the material's properties cannot be predicted directly. The material's strength suddenly drops (in a non-linear manner), and use of machinery under such conditions may pose a safety risk.

Uncontrolled loss of durability may lead to costly failures, standstills on process lines, and sometimes even to the death of those nearby when a structural component cracks. This is why information about how long and under what loading and temperature conditions a structural component can work safely is important. The fatigue damage accumulation models of materials working under low-cycle loading conditions at elevated temperatures presented in the literature are modified functions formulated to estimate the material's fatigue life at room temperature. The equations mentioned earlier can serve as an example: Manson–Coffin–Basquin, Ramberg–Osgood, and Smith–Watson–Topper. In these models, material parameters are determined independently for each of the analyzed temperatures. The process of calculating these parameters is not complicated in

itself; however, preparing the data for determining them is very expensive and time-consuming and requires specialized testing apparatus. These models are dedicated for specific loading cases and metal alloys. Due to the low number of functioning fatigue criteria in this scope, there is a justified need to create new models that will provide a more accurate description of the material cracking process, thus enabling calculation of fatigue life with greater accuracy. That is also why it this paper set out to create a new fatigue damage accumulation model that will make it possible to determine the number of cycles until failure of a material working under conditions of fatigue loads of constant amplitude at elevated temperatures with engineering accuracy.

2. Materials and Methods

2.1. Fatigue Life of EN AW-2024T3 Aluminum Alloy at Elevated Temperatures

To develop a fatigue damage accumulation model, it is indispensable to perform experimental tests. They constitute the physical basis of formulated numerical dependencies. The fatigue damage accumulation model proposed in this paper was created based on an experiment in which EN AW-2024T3 aluminum alloy samples were subjected to the action of high-amplitude fatigue loading in the form of uniaxial tension-compression and complex loading (tension-compression with simultaneous torsion) at elevated temperatures. More information about the experiment can be found in other works [4,5].

Experimental tests of fatigue life were carried out in accordance with the guidelines included in ISO 6892-1, ISO 12106: 2017, ASTM E8-04, ASTM E 606, GB/T 15248-2008, GB/T4338-2006, and (J IS) Z2201. Cylindrical and tubular test specimens (Figure 1) were made using machining. The working surfaces of the specimens were polished until satisfactory smoothness was obtained.

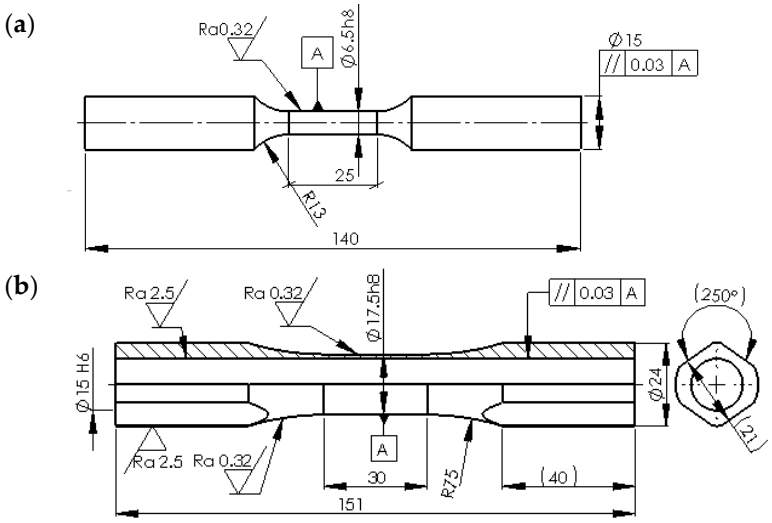

Figure 1. Diagram of test specimens for determination of the fatigue life of the material at elevated temperatures: (**a**) cylindrical specimen used in uniaxial loading tests (unit: mm) and (**b**) tubular specimen used in multiaxial loading tests (unit: mm).

The scope of performed tests covered, first of all, monotonic tests determining the influence of elevated temperatures on the mechanical properties of the EN AW-2024 T3 aerospace aluminum alloy. Table 1 presents the obtained results.

Table 1. Material parameters of the EN AW 2024 T3 alloy obtained for different temperature values [4].

T (°C)	E (GPa)	ν	σ_{yp} (MPa)	σ_{uts} (MPa)	A_5 (%)
20	72	0.33	370	536	16.7
100	64	0.33	368	516	18.4
200	53	0.33	367	500	18.8
300	52	0.33	308	418	21.6

Next, fatigue tests were carried out. Samples were subjected to uniaxial loading, periodically varying (tension-compression), until their failure at different set temperatures. Tests were performed at temperatures of 20, 100, 200, and 300 °C and at a constant value of the strain change range ε, frequency f = 1 Hz, and $R_\varepsilon = -1$. The following values of control variable ε were applied: 0.015, 0.01, 0.0095, 0.008, and 0.006. The tests were performed on three samples for every value of the control variable's range and every test temperature.

Based on the performed tests, parameters describing the process of cyclic deformation of the material (as expressed by the Ramberg–Osgood equation) at elevated temperatures were determined by the following equation:

$$\varepsilon_a = \varepsilon_a^e(T) + \varepsilon_a^p(T) = \frac{\sigma_a}{E(T)} + \left(\frac{\sigma_a}{K(T)}\right)^{1/n(T)} \quad (9)$$

where σ_a is the amplitude of normal stress induced by the action of periodic axial force, $K(T)$ and $n(T)$ are the coefficient and exponent of Ramberg-Osgood cyclic strain curve, which are dependent on temperature.

Table 2 presents the calculated parameters of the cyclic strain curve.

Table 2. Ramberg–Osgood equation parameters for the case of cyclic tension of the EN AW 2024T3 alloy at different temperature values [4].

T	20 °C	100 °C	200 °C	300 °C
$K(T)$	605.23	652.57	996.42	492.98
$n(T)$	0.0651	0.0893	0.1881	0.0602

In the next stage, parameters of the Manson–Coffin–Basquin strain-based fatigue life curve were determined. Its parameters, calculated for various temperatures, are given in Table 3.

Table 3. Coefficients and factors of the fatigue curve for the EN AW-2024T3 alloy at different temperature values [4].

$\frac{\Delta\varepsilon_{eq}}{2} = \frac{\sigma_f'(T)}{E(T)}(2N_f)^{b(T)} + \varepsilon_f'(T)(2N_f)^{c(T)}$				
T	20 °C	100 °C	200 °C	300 °C
$\sigma_f'(T)$	850 MPa	592 MPa	700 MPa	591 MPa
$b(T)$	−0.086	−0.0498	−0.083	−0.065
$\varepsilon_f'(T)$	0.22	0.43	0.168	0.25
$c(T)$	−0.462	−0.562	−0.446	−0.544

Next, samples were subjected to the action of cyclic loading with torque moment and tensile or compressive force (during loading of samples, a constant quotient of maximum longitudinal and shear strain was assumed over the course of a loading cycle: $\varepsilon_a/\gamma_a = \sqrt{3}$). In all cases, loading histories formed oriented, multi-segment loops. Their configuration and parameters are given in Figure 2. Just as in the case of uniaxial tests, the loading process was controlled by means of increments of strain tensor components.

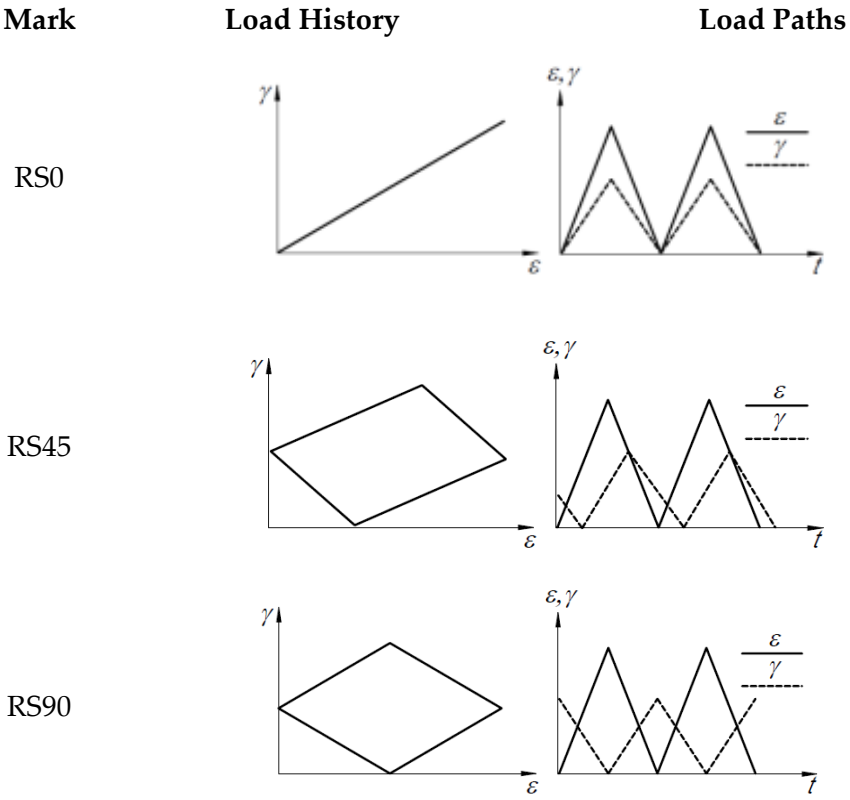

Figure 2. Evolutions of multiaxial loadings and the values of the control variable corresponding to them under the assumption of a constant quotient of maximum strains $\varepsilon_{max} = 0.003$ and $\gamma_{max} = 0.00173$ [5].

Tubular specimens (Figure 1b) were used in the experiment, and they were subjected to proportional and non-proportional tension-torsion cyclic loading with cycle asymmetry factor $R = 0$ ($\varepsilon_{min}/\varepsilon_{max}$; $\gamma_{min}/\gamma_{max}$). Fatigue tests were conducted for different combinations of axial and shear strains as well as for four temperature values: 20, 100, 200, and 300 °C. The specimen's kinematic input was controlled by means of the MTS 632.68F-08 (Eden Prairie, MN, USA) biaxial extensometer, and increments of strain components (linear and shear), averaged over a 25 mm-long segment of the measuring base, were used for this purpose. Three tests were conducted for every load with frequency of load changes $f = 1$ Hz.

The crack initiation moment was determined on the basis of the analysis of the maximum force value in the loading cycle. A 10% reduction of the force value relative to its maximum value at a given strain level was accepted as the criterion for crack initiation.

A compilation of the results of experimental tests (number of loading cycles until crack initiation) is given in Table 4.

The registered hysteresis loops for selected multiaxial loading configurations (individual loading components) have been presented in Figure 3.

Table 4. Results of experimental fatigue life tests for multiaxial loading configurations (tension/compression with torsion).

Load Path	T20		T100		T200		T300	
	N_f	$\bar{N}_f$	N_f	$\bar{N}_f$	N_f	$\bar{N}_f$	N_f	$\bar{N}_f$
RS0	6663	6376	3765	3414	1276	1432	770	894
	6638		3456		1316		992	
	5826		3020		1705		920	
RS45	6740	8287	3522	3775	2361	2015	846	1115
	7638		3911		2002		1120	
	10482		3891		1683		1379	
RS90	10290	9446	4822	4237	2100	2157	1500	1292
	8026		3556		2295		1390	
	10,023		4332		2075		987	

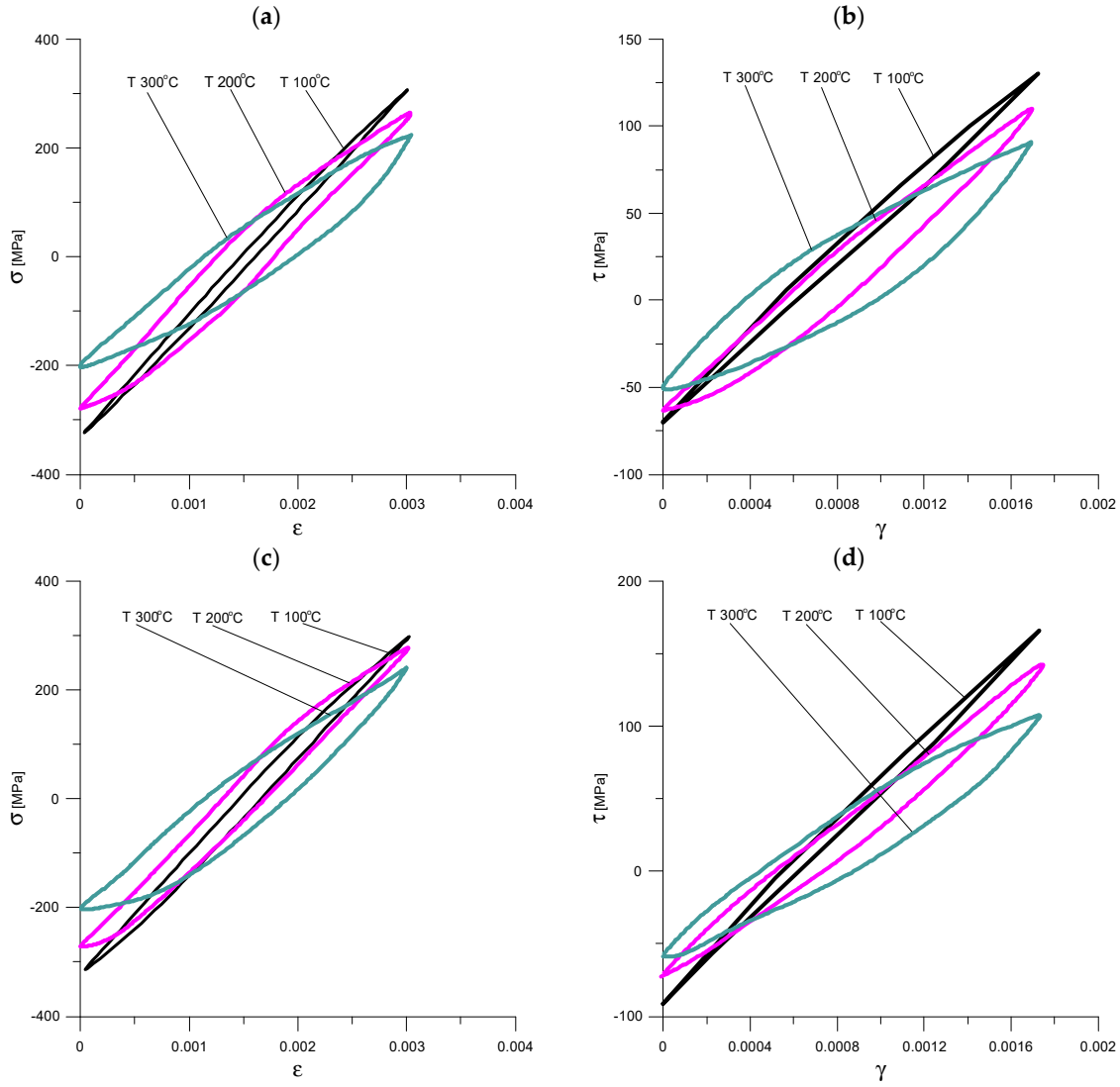

Figure 3. Hysteresis loops obtained at half of the fatigue life of the loading progression: (**a**) axial component for RS0; (**b**) non-dilatational component for various elevated temperature values for RS0; (**c**) axial component for RS45;(**d**) non-dilatational component for various elevated temperature values for RS45.

2.2. Modeling of Damage Accumulation and Fracture of Material at Elevated Temperatures

Preliminary tests based on the cyclic loading of a flat sample and observation of the amount of energy dissipating from the material due to the action of plastic strains were performed in order to investigate the fatigue damage accumulation process. The energy released as a result of fatigue loading was in the form of heat and was observed through a thermal imaging camera. Tests were performed at room temperature on the stand shown in Figure 4.

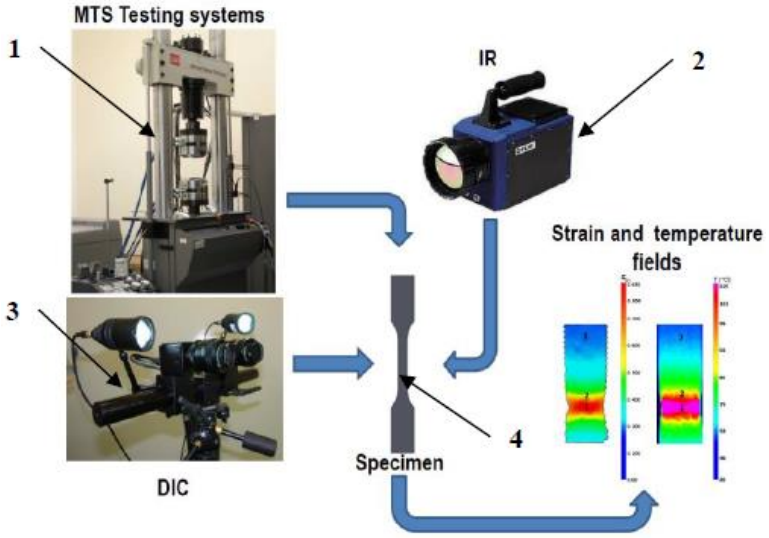

Figure 4. Test stand: 1—Fatigue testing machine, 2—thermal imaging camera IR, 3—*Aramis* video system DIC (Digital Image Correlation), 4—test sample.

During the tests, changes in the deformation fields (Aramis 4M-DIC system) and temperature fields (Cedip Titanium-IRT system) were recorded simultaneously. On their basis, areas of plastic deformation were identified and the distribution of plastic strain and energy converted into heat was determined. As can be seen in Figure 5, the temperature distribution corresponds to the strain distribution. In connection with the above, it can be assumed that the change in the temperature of the object caused by the action of external load is an indicator of damage generated during the loading process.

An example of temperature and strain fields is presented in Figure 5. Those are the fields corresponding to the localization of the plastic strain. This localization was manifested by the non-uniform temperature field and by the heterogeneity of the strain field on the specimen surface. The evolution of the temperature field due to the plastic deformation was used to determine the evolution of the field of heat dissipated by the specimen. The distribution of the heat and the plastic work on the surface of the deformed specimen was used to determine the failure mechanism.

The amount of heat emitted over the course of the tests can be related to the number of faults (damage) appearing in the material as a result of the action of external load. As the number of damages in the material increases, the object's temperature increases. Figure 6 presents the function of the maximum sample temperature at the crack initiation site as a function of test time (number of loading cycles).

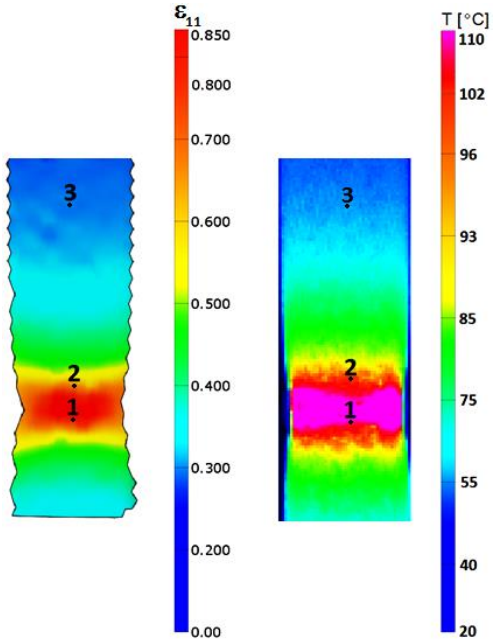

Figure 5. Fields of strain and temperature at the selected time during cyclic loading (five cycles until failure).

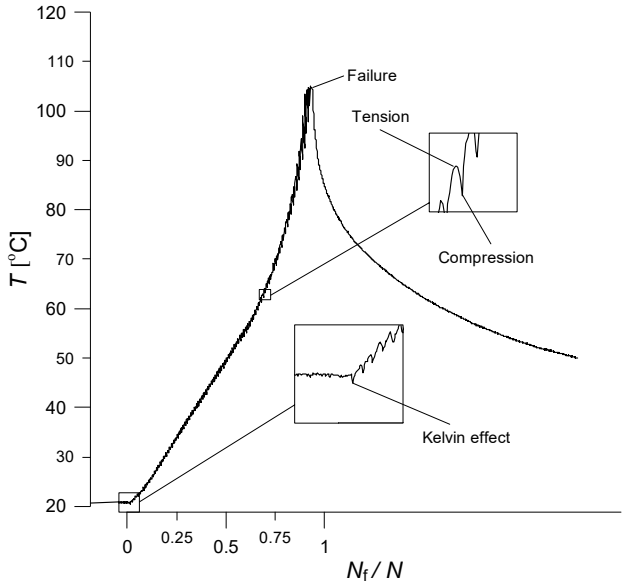

Figure 6. Evolution of temperature over the course of the process of cyclic deformation of a flat sample ENAW 2024T3.

As can be seen in the initial phase of the loading process, damage accumulated according to the linear hypothesis of damage summation. At a certain time in the loading process, there was a sharp spike in the amount of damage, observed as an increase in released thermal energy. Damage then increased exponentially. In the tensile half-cycle of loading, the object's temperature increased as a result of growing damage. Meanwhile, the compressive half-cycle slowed down the damage accumulation process, resulting in a drop of the sample's temperature.

Based on observations of fatigue cracking planes obtained over the course of experimental tests, it was noted that slip lines form first on the samples' polished surfaces under the influence of cyclic loadings at elevated temperature, even with values less than that of fatigue strength, and they transform into fatigue slip bands (numerous parallel faults) as the number of loading cycles grew (Figure 7).

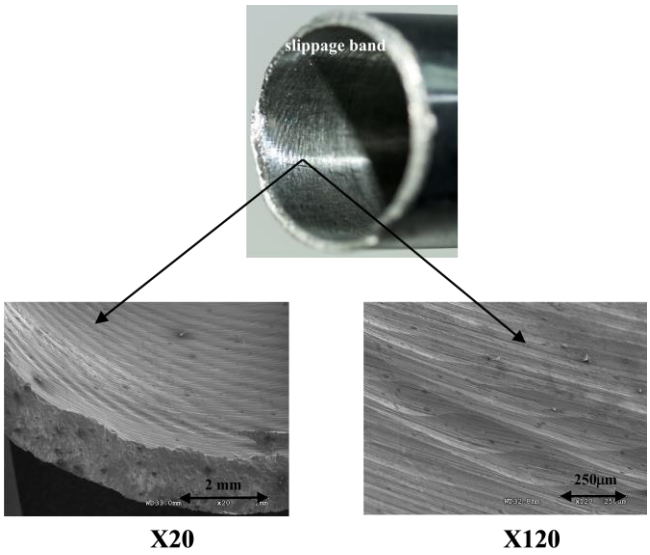

Figure 7. Slip bands (parallel faults) observed on the inner surface of a damaged tube sample (RS0—100 °C).

Similarly, as in the case of using room temperature [26], a fatigue damage accumulation criterion can be proposed based on the assumption that the material's damage state mainly depends on variable slips on physical planes and the normal stresses on these planes.

Considering the above, this paper proposes a damage accumulation model intended for the analysis of the fatigue life of constructional elements working under uniaxial and multiaxial loading conditions at elevated temperatures. This model assumes that permanent slip bands are the site of crack nucleation and defect formation [26], where crack initiation is the result of the accumulation of this damage. In this case, damage is induced by the action of the stress vector's normal component. Here, it is accepted that tensile stress in the loading cycle is responsible for generating new faults and accelerating the development of existing faults (temperature increase in loading cycle; Figure 6), while compressive stress retards the damage accumulation process (temperature drop in loading cycle; Figure 6). This fact was accounted for in the definition of the damage state variable $\mathrm{d}\omega_{\mathrm{n}}$.

The presented law of damage accumulation induced by plastic strains under elevated temperature conditions was linked to the stress-based damage accumulation function Ψ_{p}, the value of which is dependent on the value of normal stresses σ_{n}, damage state variable ω_{n} on the physical plane, and temperature T. The increment of the damage state variable on the physical plane $\mathrm{d}\omega_{\mathrm{n}}$, as caused by the development of plastic strains at elevated temperature T, was made dependent on the increment of plastic shear strains $\mathrm{d}\gamma_{\mathrm{n}}{}^{\mathrm{p}}$ on the same plane [27], namely:

$$\begin{cases} \mathrm{d}\omega_n(\boldsymbol{\sigma}, \mathrm{d}\boldsymbol{\varepsilon}, T) = A_{\mathrm{p}}(T)\, \Psi_{\mathrm{p}}(\sigma_n, \omega_n, T) \left|\mathrm{d}\gamma_n^{\mathrm{p}}\right| & \text{for } \sigma > 0 \text{ i } \mathrm{d}\varepsilon > 0 \\ \mathrm{d}\omega_n(\boldsymbol{\sigma}, \mathrm{d}\boldsymbol{\varepsilon}, T) = 0 & \text{for } \sigma \leq 0 \text{ i } \mathrm{d}\varepsilon \leq 0 \end{cases} \tag{10}$$

where $A_{\mathrm{p}}(T)$ is the material variable describing the evolution of the material's plastic properties depending on the actual stress state and temperature. In numerical simulations, the following values of parameter A_{p} were accepted: $A_{\mathrm{p}}(20\ ^{\circ}\mathrm{C}) = 0.55$; $A_{\mathrm{p}}(100\ ^{\circ}\mathrm{C}) = 1.4$; $A_{\mathrm{p}}(200\ ^{\circ}\mathrm{C}) = 1.8$; and $A_{\mathrm{p}}(300\ ^{\circ}\mathrm{C}) = 1.95$.

The damage accumulation mechanism described by this law is presented in Figure 8.

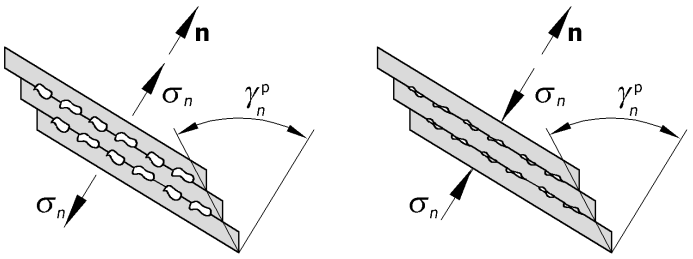

Figure 8. Generation of defects on the physical plane by slip band [22].

Similar to the dependencies presented in the work [26], the damage accumulation function Ψ_p can be proposed in the following form:

$$\Psi_p(\sigma_n, \omega_n, T) = \left(1 - \frac{1}{3} R_\sigma(\sigma_n, \omega_n, T)\right)^{1/c(T)} \tag{11}$$

where R_σ is the stress function of cracking given by the condition of maximum normal stresses, which is dependent on the test temperature:

$$R_\sigma(\sigma_n, \omega_n, T) = \frac{\sigma_n}{\sigma_c(\omega_n, T)} \tag{12}$$

$c(T)$ is the exponent present in the Manson–Coffin–Basquin equation, which is also dependent on temperature (values of parameter $c(T)$ used in numerical simulations are given in Table 3).

The crack initiation criterion can be written in the form of the condition of maximum normal stresses (linked to the physical plane), namely:

$$R_{f\sigma} = \max_{(\mathbf{n})} R_\sigma(\sigma_n, \omega_n, T) = \max_{(\mathbf{n})} \left(\frac{\sigma_n}{\sigma_c(\omega_n, T)}\right) = 1 \tag{13}$$

where $R_{f\sigma}$ is the stress cracking coefficient dependent on the state of stress and damage in the material as well as on the test temperature T, and σ_c is the actual value of normal failure stresses for the material at the given temperature, which is dependent on the damage state variable and temperature, namely:

$$\sigma_c(\omega_n, T) = \sigma_{c0}(T)(1 - \omega_n), \tag{14}$$

where $\sigma_{c0}(T)$ is the critical stress for undamaged material, which is dependent on temperature. The value of parameter $\sigma_{c0}(T)$ can be equated with the value of the coefficient of the Manson–Coffin fatigue life curve $\sigma_f'(T)$. Critical stress values according to Table 3 were used to calculate the accumulation of fatigue damage by means of the proposed model.

An additional cracking condition should also be introduced, in which it is accepted that crack initiation will occur when the damage state variable induced by plastic strains on any physical plane reaches critical value, that is:

$$\max_{(\mathbf{n})} \omega_n = 1. \tag{15}$$

At that moment, the material has no strength ($\sigma_c = 0$).

In the presented model, stress and strain values were determined independently for each test temperature by using the generalized Hooke's law, the Huber-von Mises yield criterion, the gradient flow law, and Mroz–Garud multiple-surface material hardening model associated with the yield criterion. They are an integral part of the numerical model of damage accumulation, making it possible to determine stress and strain state in any loading state [28].

When estimating the material's fatigue life, the principle of additivity of components of elastic and plastic strain increment tensors was adopted. Increments of elastic strain were determined by

means of the generalized Hooke's law, and increments of plastic strain were calculated by means of the gradient flow law, associated with the yield surface, namely (T = const):

$$\mathrm{d}\varepsilon_{ij} = \frac{1+\nu(T)}{E(T)}\mathrm{d}\sigma_{ij} - \frac{\nu(T)}{E(T)}\mathrm{d}\sigma_{kk}\delta_{ij} + \mathrm{d}\lambda(T)\frac{\partial f(T)}{\partial \sigma_{ij}}, \tag{16}$$

where both the proportionality coefficient $\mathrm{d}\lambda$ and the elasticity constants E and ν are dependent on temperature. In numerical simulations, the values of parameters determined in monotonic tensile tests were used according to Table 1. The material's hardening curve was plotted according to the parameters given in Table 2.

Yield surface $f = 0$ was determined using the Huber-von Mises criterion:

$$f = \frac{3}{2}\left(s_{ij} - \alpha_{ij}\right)\left(s_{ij} - \alpha_{ij}\right) - R(T)^2 = 0, \tag{17}$$

where $R(T)$ defines the temperature-dependent size of the yield surface.

3. Results

Simulations of the fatigue life of the aerospace aluminum alloy within the range of uniaxial loads (tension-compression) at elevated temperatures were conducted for the modified Manson-Coffin-Basquin model (Equation (1)), semi-empirical model S-S_1 (Equation (2)), and the proposed approach S-S_2 (Equation (10)). Damage accumulation simulations were carried out for four different temperatures and five strain levels. The results of the simulations are provided in Table 5.

Table 5. Experimental data and results of numerical simulations of fatigue damage accumulation for uniaxial loads at elevated temperatures.

Strain Level	Calculations N_f (cycle)			Exp. N_f
	M-C-B	S-S_1	S-S_2	(cycle)
		20 °C		
0.015	575	734	534	572
0.01	2510	3358	2181	2704
0.0095	3205	4151	3529	4156
0.008	6724	6717	5231	6458
0.006	12,838	12,316	14,164	14,597
		100 °C		
0.015	695	452	424	464
0.01	3100	2135	2252	2164
0.0095	2200	3282	3381	3209
0.008	6250	5098	5308	5168
0.006	12,000	11,524	10,630	10,755
		200 °C		
0.015	550	301	368	355
0.01	1955	1424	1589	1679
0.0095	3700	2188	2315	2178
0.008	4960	3399	4527	4435
0.006	9520	7683	9119	8328
		300 °C		
0.015	250	151	218	225
0.01	850	712	509	464
0.0095	1056	1094	865	870
0.008	1623	1700	1867	1882
0.006	4450	3842	3870	3775

Figure 9a presents the evolution of the damage state variable over the course of the fatigue loading process, plotted based on Equation (10) for the analyzed levels of temperature and strain $\varepsilon_a = 0.015$. As can be seen in its evolution, the fatigue damage accumulation process progresses in a near-linear manner in the first loading stage until it reaches a certain limit state, and after this limit state is crossed, there is a sudden spike in damage. This was confirmed by thermograms (Figure 9b), which show a sudden temperature increase in the final phase of periodic loading. The characters of the fatigue damage accumulation process and of the evolution of the sample's temperature were similar over the course of cyclic loading. It can be surmised that the object's temperature may be an indicator of the number of damage accumulated over the course of the material loading process.

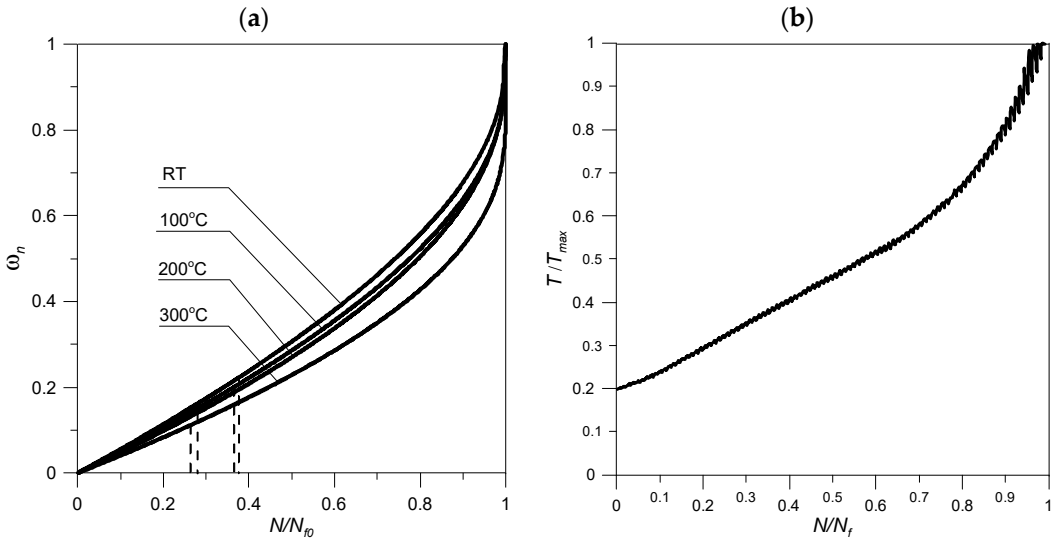

Figure 9. (**a**) Evolution of the damage state variable over the course of the action of fatigue load for different temperatures and strain levels $\varepsilon_a = 0.015$. (**b**) Evolution of sample temperature over the course of cyclic loading at RT–Room Temperature.

Temperature influences the rate at which the material subjected to the action of cyclic loads reaches the state of "damage saturation". Samples loaded at 300 °C reached the limit state after working 0.26 of the number of cycles until failure, while at room temperature, this state was reached after 0.38 of the number of cycles until failure. This state can be explained by the fact that movement of dislocations is facilitated as temperature increases, since they do not encounter obstacles that could slow them down on their path due to the elevated mobility of atoms. After crossing the "limit" state, further damage accumulation progresses exponentially. Microcracks appear in the material, leading to the material's decohesion as they are joined.

Figure 10 presents a comparison of numerical calculations of fatigue life (for the modified Manson-Coffin-Basquin model (Equation (1)), semi-empirical model S-S_1 (Equation (2)), and the proposed approach S-S_2 (Equation (10)) with experimental data for uniaxial tension-compression of ENAW2024T3 aluminum alloy samples at elevated temperature: (a) 20 °C; (b) 100 °C; (c) 200 °C, (d) 300 °C.

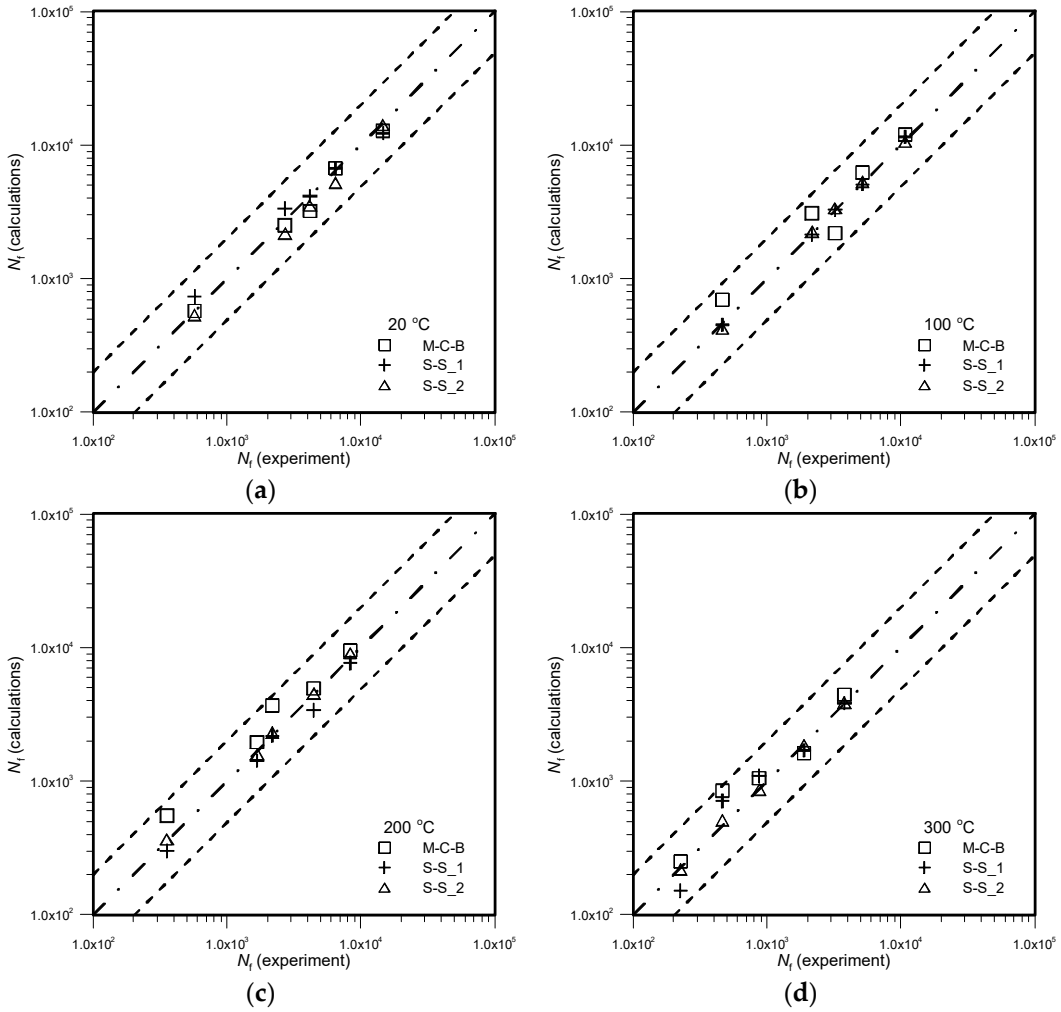

Figure 10. Comparison of numerical simulations of fatigue life with experimental data for uniaxial tension-compression of ENAW2024T3 aluminum alloy samples at elevated temperature: (**a**) 20 °C; (**b**) 100 °C; (**c**) 200 °C, (**d**) 300 °C.

Next, the proposed fatigue damage accumulation model was also verified for the case of multiaxial loads. The results of original experimental tests performed on the EN AW-2024T3 aerospace aluminum alloy were used for this purpose [5]. Figure 11 presents normalized evolutions of the damage state variable, plotted for load paths RS0 and RS90 at the analyzed temperature. A comparison between the results of experimental tests and of numerical simulations using the proposed SS2 approach (Equation (10)) and the SS1 semi-empirical model (Equation (2)) described in Reference [5] is given in Figure 12 and in Table 6.

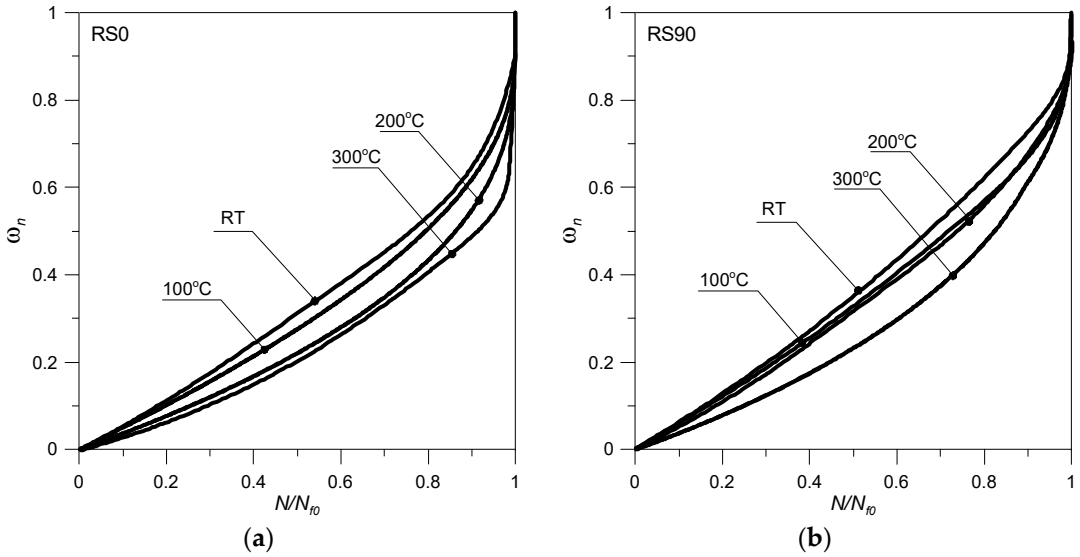

Figure 11. Evolution of damage state variable normalized with respect to cycles until crack initiation at the analyzed temperature for load path: (**a**) RSO; (**b**) RS90.

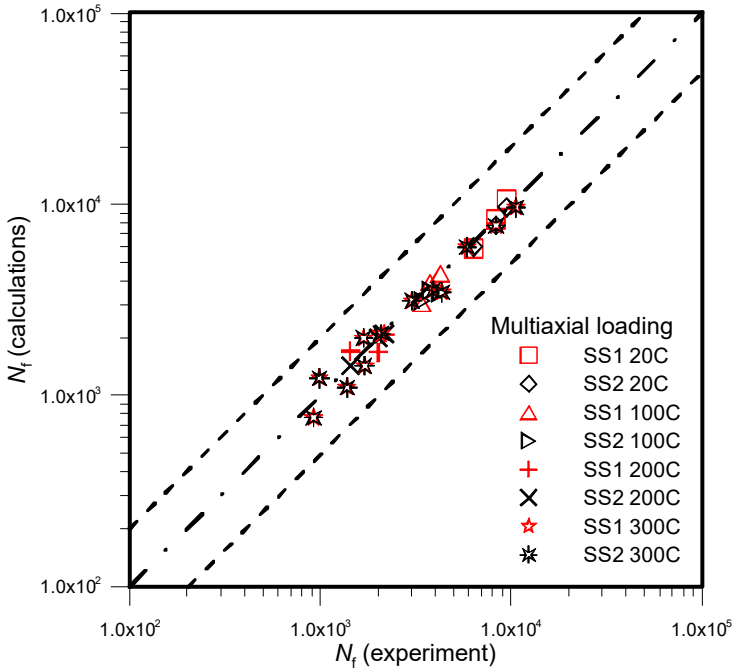

Figure 12. Comparison of the results of numerical simulations (strain-based approach) with experimental data for the EN AW-2007 aluminum alloy for complex loading histories.

Table 6. Comparison of the results of numerical simulations using the SS1 model (Szusta Seweryn 2015) and SS2 model (Equation (10)) and experimental tests of the number of cycles N_f for different loading paths (EN AW-2024 T3).

Load Path	Calculations N_f (cycle)		Exp. N_f
	SS1	SS2	(cycle)
	20 °C		
RS0	5876	5983	6376
RS45	8347	7739	8287
RS90	10,583	9655	9446
	100 °C		
RS0	3020	3122	3414
RS45	3891	3538	3775
RS90	4332	3459	4237
	200 °C		
RS0	1705	1426	1432
RS45	1683	1995	2015
RS90	2075	2103	2157
	300 °C		
RS0	920	764	894
RS45	1379	1099	1115
RS90	987	1230	1292

The conducted simulations indicate good consistency between results obtained using the proposed strain-based model and the authors' original experimental results, within the scope of both uniaxial and complex loading.

4. Conclusions

This paper presents an approach that makes it possible to estimate the fatigue life of materials working under conditions of cyclic loading at elevated temperatures. An undoubted advantage of the model is its capability of accounting for the loading history in the fatigue damage accumulation process. This is done when determining stress or strain tensor components depending on the method of effecting force (force/displacement). The tests verifying the developed model show that, in the initial loading phase, as a result of the action of cyclic loads, damage accumulates gradually with every cycle of high-amplitude loading until the material reaches a certain limit state. After this state is exceeded, the "damage density" is high enough that the material is no longer able to safely carry the load applied to it. The process related to the appearance of microcracks in the material then occurs, and this leads to a sharp rise in damage during further loading. After that, faults increase exponentially until macrocracks form, leading to decohesion of the material. Elevated temperatures foster damage accumulation by facilitating the yielding of the material; dislocations can move more easily within the material. Moreover, the material's temperature changes the character of cracking and the time until failure.

Author Contributions: J.S. was the author of the concept of the article, made calculations, and analyzed the results. A.S. was a scientific consultant.

Funding: The investigation described in this paper is part of the research project no. G/WM/5/2017 Sponsored by the Polish National Science Centre and realized in Bialystok University of Technology.

Conflicts of Interest: The authors declare no conflicts of interest.

References

1. Tomczyk, A.; Seweryn, A.; Gradzka-Dhalke, M. The effect of dynamic recrystallization on monotonic and cyclic behaviour of Al-Cu-Mg alloy. *Materials* **2018**, *11*, e874. [CrossRef] [PubMed]
2. Juijerm, P.; Altenberger, I. Effect of temperature on cyclic deformation behavior and residual stress relaxation of deep rolled under-aged aluminium alloy AA6110. *Mater. Sci. Eng.* **2007**, *452–453*, 475–482. [CrossRef]
3. Karakas, O.; Szusta, J. Monotonic and Low Cycle Fatigue Behaviour of 2024-T3 Aluminium Alloy between Room Temperature and 300 °C for Designing VAWT Components, Fatigue. *Fract. Eng. Mater. Struct.* **2016**, *39*, 95–109.
4. Szusta, J.; Seweryn, A. Damage accumulation modeling under uniaxial low cycle fatigue at elevated temperatures. *Eng. Fail. Anal.* **2015**, *56*, 474–483. [CrossRef]
5. Szusta, J.; Seweryn, A. Experimental study of the low-cycle fatigue life under multiaxial loading of aluminum alloy EN AW-2024-T3 at elevated temperatures. *Int. J. Fatigue* **2017**, *96*, 28–42. [CrossRef]
6. Samec, A.; Potrc, I.; Sraml, M. Low cycle fatigue of nodular cast iron used for railway brake discs. *Eng. Fail. Anal.* **2011**, *18*, 1424–1434. [CrossRef]
7. Pevec, M.; Oder, G.; Potrc, I.; Sraml, M. Elevated temperature low cycle fatigue of grey cast iron used for automotive brake discs. *Eng. Fail. Anal.* **2014**, *42*, 221–230. [CrossRef]
8. Li, Z.; Han, J.; Li, W.; Pan, L. Low cycle fatigue behavior of Cr–Mo–V low alloy steel used for railway brake discs. *Mater. Des.* **2014**, *56*, 146–157. [CrossRef]
9. Ishii, T.; Fukaya, K.; Nishiyama, Y.; Suzuki, M.; Eto, M. Low cycle fatigue properties of 8Cr-2WVTa ferritic steel at elevated temperatures. *J. Nucl. Mater.* **1998**, *258–263*, 1183–1186. [CrossRef]
10. Mariappan, K.; Shankar, V.; Sandhya, R.; Laha, K. Low cycle fatigue design data for India-specific reduced activation ferritic-martensitic (IN-RAFM) steel. *Fusion Eng. Des.* **2016**, *104*, 76–83. [CrossRef]
11. Shankar, V.; Kumar, A.; Mariappan, K.; Sandhya, R.; Laha, K.; Bhaduri, A.K.; Narasaiah, N. Occurrence of dynamic strain aging in Alloy 617M under low cycle fatigue loading. *Int. J. Fatigue* **2017**, *100*, 12–20. [CrossRef]
12. Nagode, M.; Zingsheim, F. An online algorithm for temperature influenced fatigue–life estimation: Strain–life approach. *Int. J. Fatigue* **2004**, *26*, 155–161. [CrossRef]
13. Nagode, M.; Hack, M. An online algorithm for temperature influenced fatigue life estimation: Stress–life approach. *Int. J. Fatigue* **2004**, *26*, 163–171. [CrossRef]
14. Schlesinger, M.; Seifert, T.; Preussner, J. Experimental investigation of the time and temperature dependent growth of fatigue cracks in Inconel 718 and mechanism based lifetime prediction. *Int. J. Fatigue* **2017**, *99*, 242–249. [CrossRef]
15. Maderbacher, H.; Oberwinkler, B.; Gänser, H.-P.; Tan, W.; Rollett, M.; Stoschka, M. The influence of microstructure and operating temperature on the fatigue endurance of hot forged Inconels 718 components. *Mater. Sci. Eng. A* **2013**, *585*, 123–131. [CrossRef]
16. Tunthawiroona, P.; Lib, Y.; Koizumia, Y.; Chibaa, A. Strain-controlled iso-thermal fatigue behavior of Co–29Cr–6Mo used for tooling materials in Al die casting. *Mater. Sci. Eng. A* **2017**, *703*, 27–36. [CrossRef]
17. Gopinath, K.; Gogia, A.K.; Kamat, S.V.; Balamuralikrishnan, R.; Ramamurty, U. Low cycle fatigue behaviour of a low interstitial Ni-base superalloy. *Acta Mater.* **2009**, *57*, 3450–3459. [CrossRef]
18. He, Y.H.; Chen, L.J.; Liaw, P.K.; McDaniels, R.L.; Brooks, C.R.; Seeley, R.R.; Klarstrom, D.L. Low-cycle fatigue behavior of HAYNES HR-120 alloy. *Int. J. Fatigue* **2002**, *24*, 931–942. [CrossRef]
19. Kim, Y.-J.; Ho, J. High temperature fatigue resistance of an ACI HH50-type cast austenitic stainless steel. *Mater. Sci. Eng.* **2010**, *527*, 5415–5420. [CrossRef]
20. Pavlou, D.G. Creep life prediction under stepwise constant uniaxial stress and temperature conditions. *Eng. Struct.* **2001**, *23*, 656–662. [CrossRef]
21. Grell, W.A.; Niggeler, G.H.; Groskreutz, M.E.; Laz, P.J. Evaluation of creep damage accumulation models: Considerations of stepped testing and highly stressed volume. *Fatigue Fract. Eng. Mater. Struct.* **2007**, *30*, 689–697. [CrossRef]
22. Altenberger, I.; Nalla, R.K.; Sano, Y.; Wagner, L.; Ritchie, R.O. On the effect of deep-rolling and laser-peening on the stress-controlled low- and high-cycle fatigue behavior of Ti–6Al–4V at elevated temperatures up to 550 °C. *Int. J. Fatigue* **2012**, *44*, 292–302. [CrossRef]

23. Heckel, T.K.; Christ, H.J. Thermomechanical Fatigue of the TiAl Intermetallic Alloy TNB-V2. *Exp. Mech.* **2009**, *50*, 717–724. [CrossRef]
24. Chen, L.J.; Eang, Z.G.; Yao, G.; Tian, J.F. 1The influence of temperature on low cycle fatigue behavior of nickel base superalloy GH4049. *Int. J. Fatigue* **1999**, *21*, 791–797. [CrossRef]
25. Bar-Cohen, Y. *High Temperature Materials and Mechanisms*; CRC Press: Boca Raton, FL, USA, 2017.
26. Szusta, J.; Seweryn, A. Low-cycle fatigue model of damage accumulation—The strain approach. *Eng. Fract. Mech.* **2010**, *77*, 1604–1616. [CrossRef]
27. Szusta, J.; Seweryn, A. Fatigue damage accumulation modelling in the range of complex low-cycle loadings—The strain approach and its experimental verification on the basis of EN AW-2007 aluminum alloy. *Int. J. Fatigue* **2011**, *33*, 255–264. [CrossRef]
28. Seweryn, A.; Buczynski, A.; Szusta, J. Damage accumulation model for low cycle fatigue. *Int. J. Fatigue* **2008**, *30*, 756–765. [CrossRef]